International Journal of Environmental Science and Technology (2025) 22:4369–4384
https://doi.org/10.1007/s13762-024-06127-0

ORIGINAL PAPER

Tungsten oxide embellished graphitic carbon nitride for dye industrial wastewater remediation using visible light

V. S. Rao[1] · A. Sharma[2] · S. P. Nehra[1]

Received: 5 July 2024 / Revised: 4 September 2024 / Accepted: 8 October 2024 / Published online: 29 October 2024

Abstract

A process showing potential for slowing down the quick recombination of photogenerated electron-holes and enhancing the dispersion of charges produced by photocatalytic reaction during photodegradation processes is coupling of semiconductor photocatalysts. In the current study, tungsten oxide embellished graphitic carbon nitride (WCN) nanocomposites have been prepared. Three different photocatalytic composites of tungsten oxide and gCN in the mass ratios of 1:1, 2:1, and 3:1, denoted WCN1, WCN2, and WCN3, were created for the methylene blue (MB) and methyl orange (MO) photodegradation. Thermogravimetric analysis (TGA), X-ray photoelectron spectroscopy (XPS), Fourier-transform infrared spectroscopy (FTIR), X-ray diffraction (XRD), and scanning electron microscopy (SEM) were adapted to characterize the morphological, structural and optical features of the treated photocatalyst. Graphitic carbon nitride (gCN), a metal-free photocatalyst, has drawn considerable interest because of its possible use in photocatalytic environmental pollution treatment. The findings show that, rather than changing the sample crystalline structure, this extensively disperses gCN to increase its surface area. The combined photocatalytic degradation rate of MB after 150 min in visible light (500–800 nm) was 52.46% for gCN, 86.4% for WCN1, 98.8% for WCN2, and 91.2% for WCN3. For methyl orange, the generated materials' photocatalytic activity was examined. The analysis outcome reveals astonishing deterioration values for WCN1 (72.9%), WCN2 (89.7%), and WCN3 (83.6%), respectively. For five cycles, the hybrid photocatalyst yielded consistent photodegradation results and check their Total organic carbon reduction in the wastewater after treatment. It has been observed that W_2O_6/gCN is promising photocatalyst for dye industrial wastewater remediation using visible light.

Editorial responsibility: S. Mirkia.

✉ A. Sharma
anshushsharda@gmail.com

S. P. Nehra
nehrasp@gmail.com

[1] Center of Excellence for Energy and Environmental Studies, Deenbandhu Chhotu Ram University of Science and Technology, Murthal 131039, India

[2] Department of Physics, School of Engineering and Technology, Central University of Haryana, Mahendragarh 123031, India

Graphical Abstract

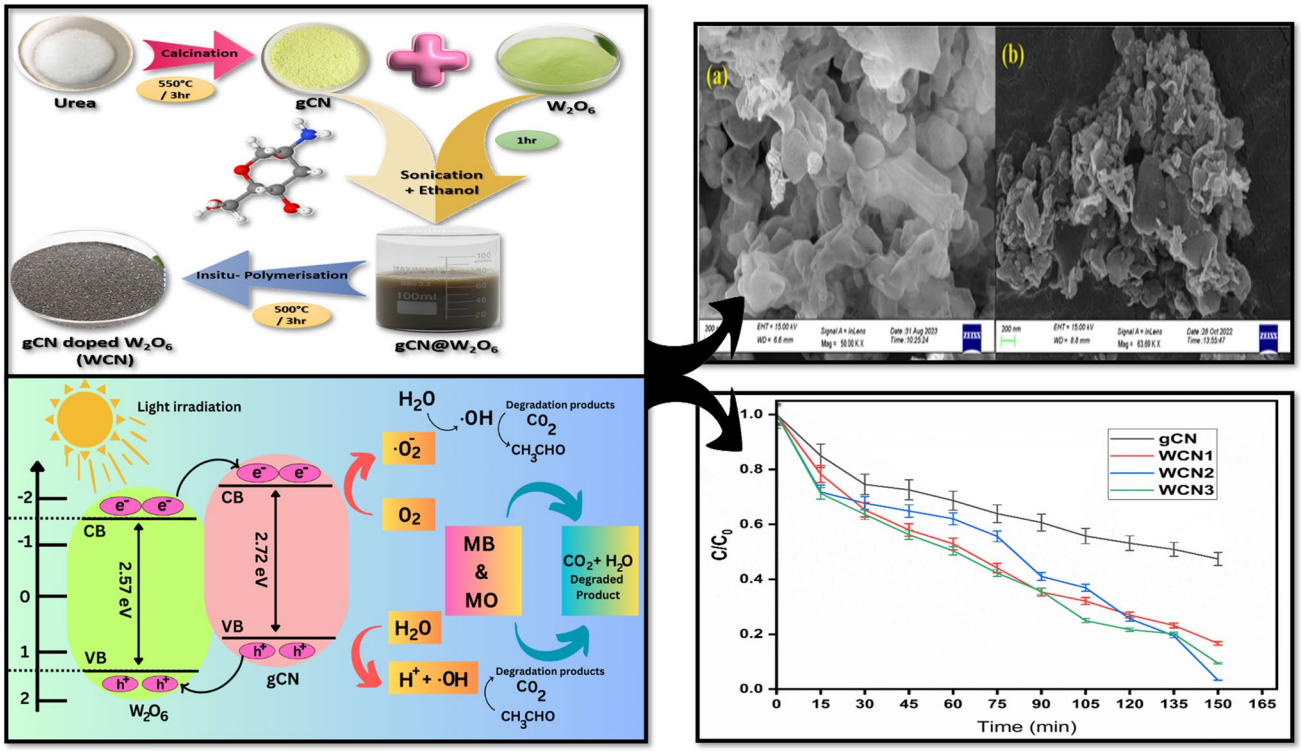

Keywords Photoreduction · gCN · W_2O_6 · Photocatalyst · Heterojunction · Wastewater remediation

Introduction

All living things depend on water as a resource, and the health and wellbeing of human societies and ecosystems are directly impacted by the quality of water. Nonetheless, water pollution has grown to be a significant worldwide concern as a result of fast industrialization, urbanization, and population expansion (Sibiya et al. 2022). Water bodies are deteriorating due to the presence of several pollutants, like heavy metals, organic dyes, and new pollutants, endangering the supply of clean and safe water (Yesmin et al. 2022). Innovative and sustainable methods are therefore desperately needed to combat water pollution and clean up contaminated water sources (Ji et al. 2021). A potential method for cleaning up water is called photocatalysis, which uses light energy to start chemical reactions that turn dangerous toxins into benign byproducts (Rao et al. 2024a). The development of sophisticated photocatalytic materials has recently been the focus of substantial research in an effort to improve this process effectiveness and efficiency (Alaghmandfard and Ghandi 2022). Because of its remarkable photocatalytic qualities, the combination of W_2O_6 (tungsten trioxide) with graphitic carbon nitride (gCN) has gained a great deal of interest among these materials.

In the last few years, various semiconducting materials, such as TiO_2, ZnO, and CdS, have been thoroughly investigated for their photocatalytic qualities (Das et al. 2017). Yet many materials have some drawbacks that limit their photocatalytic efficacy, namely broad bandgaps and quick charge carrier recombination. As a result, scientists are now focusing on creating novel photocatalytic materials with enhanced characteristics (Liu et al. 2021b). Owing to its superior electrical and optical properties, tungsten trioxide, a transition metal oxide semiconductor, has garnered significant interest among the photocatalysis community (Tomer et al. 2017). Because of its very narrow bandgap and ability to absorb visible light, tungsten oxide is a desirable photocatalyst for applications involving visible light (Tripathi and Narayanan 2018). Additionally, transitional metal oxides has various oxidation states and good stability, which makes it easier for reactive oxygen species (ROS) to be produced during photocatalytic reactions (Rattan Paul and Nehra 2021).

Graphitic carbon nitride (gCN) possesses a band gap of approximately 2.7 eV, enabling visible light absorption for

photocatalytic processes such as water splitting, hydrogen production, and environmental remediation. Its chemical stability under light irradiation and in various environments, including acidic and basic conditions, ensures long-term durability and practical applicability (Sundaram et al. 2017). The semiconducting properties of gCN can be tuned through doping or forming composites, making it versatile for use in electronic and optoelectronic devices. gCN exhibits efficient charge separation, minimizing electron–hole recombination and enhancing photocatalytic performance (Tanzifi et al. 2023). Composed of earth-abundant carbon and nitrogen, it is an environmentally sustainable material with biocompatibility, suitable for biomedical applications like drug delivery and biosensors. Its porous structure offers a high surface area advantageous for gas adsorption and heterogeneous catalysis. Synthesis of g-CN from low-cost precursors such as urea, melamine, or cyanamide contributes to its economic viability for large-scale production. Additionally, its thermal stability up to ~ 600 °C makes it suitable for high-temperature applications.

Even though gCN independently show encouraging photocatalytic qualities, their combining to form a hybrid nanocomposite has a synergistic effect that increases both of their total photocatalytic activity (Bahuguna et al. 2018). This synergism results from the special qualities and traits of each component, which improves charge separation, increases the range of light absorption, and strengthens redox reactions (Paul et al. 2022). W_2O_6 serves as an electron acceptor and gCN as an electron donor in the W_2O_6/gCN hybrid. Besides this, the hybrid structure close proximity and effective electrical interaction between W_2O_6 and gCN promote the quick migration of charge carriers over the interface. When compared to the separate components, this interfacial synergy improves charge separation and transportation, leading to greater photocatalytic efficiency and performance (Paul et al. 2020a). Utilizing the W_2O_6/gCN hybrid nanocomposite increased photocatalytic activity for water remediation applications requires the successful production of the material. A variety of procedures, including as co-precipitation, hydrothermal, and sol–gel approaches, have been used to create the hybrid material (Kamarasu et al. 2022).

Optimizing the efficacy of the transitional metal oxide and gCN hybrid nanocomposite in water remediation requires an understanding of its photocatalytic processes (Arora et al. 2023). A number of processes are participated in the photocatalytic process, such as redox reactions, charge creation, separation of charges and absorption of light (Mendoza-Sánchez et al. 2013). The hybrid nanocomposite total photocatalytic effectiveness is influenced by the synergistic effects of W_2O_6 and gCN, which are crucial in each of these phases (Nabeel et al. 2023; Ngare et al., 2019). When photons with energy above the hybrid material bandgap are absorbed during photocatalysis, electron–hole pairs are produced in both transitional metal oxide and gCN (Li et al. 2020; Tripathi et al. 2020). There is a greater chance of redox interactions with water pollutants because of the photogenerated electrons and holes migrating to their appropriate energy levels and the effective electron transfer from gCN to W_2O_6. This process also makes charge separation easier and recombination less likely (Chand and Mondal 2023)(Mo et al. 2019). Furthermore, the hybrid nanocomposite high surface area and porous nature offer a wealth of active sites for pollutant adsorption, which accelerates the process of photocatalytic destruction (Tian et al. 2021). The potential of transitional metal oxide and gCN hybrid nanocomposites for water remediation seems bright in spite of these obstacles (Menon et al. 2021). It is anticipated that continued research into the limitations found and new directions for improving the material photocatalytic capabilities would produce insightful discoveries and creative solutions (Huang et al. 2022). Furthermore, developments in materials science and nanotechnology will probably help create more effective and long-lasting photocatalysts, which will accelerate the development of water remediation technologies (Liu et al. 2021a).

Herein, we employ the combination of gCN, W_2O_6 to design W_2O_6@gCN in a hybrid nanocomposite presents a highly attractive and viable solution for enhanced photocatalytic activity in water remediation. The synergistic effects arising from their unique properties and efficient electron transfer processes result in improved charge separation and transportation, leading to superior photocatalytic efficiency compared to their individual counterparts. The phase purity, chemical composition, and morphology of the gCN sample and modified W_2O_6@gCN (WCN) synthesized through the two-step process sonication followed by in-situ polymerization process were investigated. The powder XRD method was utilized to investigate the fabricated W_2O_6@gCN phase integrity. To see if gCN alters its molecular structure, the FTIR spectra of gCN produced with W_2O_6 and W_2O_6@gCN were examined. Under visible light irradiation, Examining the photocatalytic activity involved breaking down of methylene blue (MB) and methylene orange (MO), two prominent contaminants in the effluent water of textile and tanning industry. The development and application of the W_2O_6@gCN hybrid nanocomposite offer a promising avenue for sustainable water treatment, contributing to the preservation of clean and safe water resources for present and future generations. With continued research and innovation, this cutting-edge photocatalytic material holds the potential to revolutionize water remediation technologies and play a pivotal role in mitigating the global water pollution crisis.

Materials and methods

Chemicals

Analytical-grade urea was provided by Sigma Aldrich with 99.9% purity and used exactly as directed. 99.9% pure tungsten oxide was purchased from Sigma Aldrich. The dyes methylene orange (MO) and methylene blue (MB) and were used without further purification. Fisher Scientific was the source of both products (India). Ethanol solution was supplied by Fisher Scientific with the purity of 99.9% and was utilized to dissolve the precursors. Throughout the experiment, deionized water (DI) has been utilized to prevent interference from other ions.

Synthesis of gCN

Thermal polymerization technique was used to create the gCN photocatalyst from urea. Five grams of each precursor were added to a 50-ml crucible and covered with aluminum foil to yield bulk gCN. Subsequently, the crucible filled with compound was placed into the muffle furnace then heat to 550 °C for three hours while being exposed to air at a rate of 15 °C per minute (Rao et al. 2024b). It was not handled until it attained the surrounding environment's temperature. The resulting light pale yellow powdered sample of gCN produced from urea has been ground into a fine powder.

Preparation of gCN/W_2O_6 composites

The gCN@W_2O_6 photocatalytic material was created using a straightforward sonication followed by thermal polymerization process employing urea and tungsten oxide as depicted in Fig. 1. Moreover, various ratio arrangements of gCN/W_2O_6 (WCN) were produced. The aforementioned process was used to create 0.6 g of gCN and 0.6 g W_2O_6 in a 1:1 mass ratio (WCN1), 0.6 g of gCN and 0.3 g W_2O_6 (WCN2), and 0.6 g of gCN and 0.2 g W_2O_6 (WCN3) in 2:1 and 3:1 mass ratio, accordingly. The gCN produced from urea and W_2O_6 doped composites of a mixture of (1:1), (2:1), and (3:1) will now be referred to as WCN1, WCN2, and WCN3.

Characterization of photocatalysts

Employing a range of analytical methods, the physical properties, chemical makeup, and photochemistry of the gCN, W_2O_6, and W_2O_6@gCN photocatalytic materials were assessed. A 400–4000 cm^{-1} FTIR (Fourier transform infrared) spectrophotometer was employed to determine the structural purity of the gCN. Powder X-ray diffraction of the produced sample was carried out using a Bruker D8 discover X-ray diffractometer (XRD). The structure and morphology of the photocatalyst were investigated using the Zeiss Gemini SEM 500 Thermal field emission microscope and field emission scanning electron microscopy (FE-SEM). Measurements of thermogravimetric analysis (TGA) were performed using a TGA HiRes1000 RT to 1100 °C equipment in the 10–800 °C temperature variation, heating at an intensity of 10 °C min^{-1} in an Ar environment.

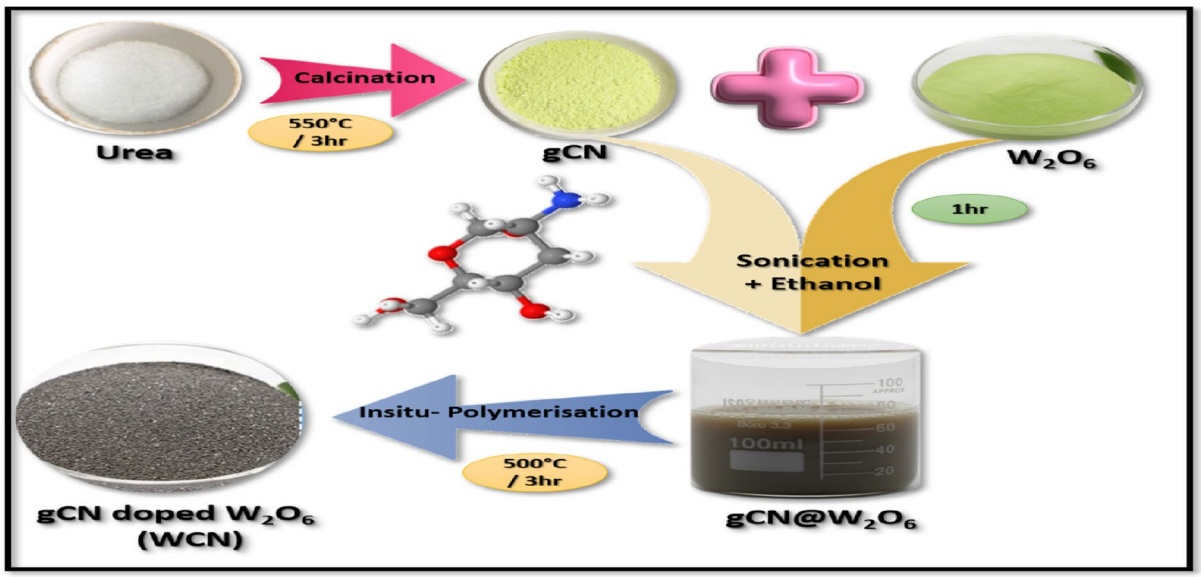

Fig. 1 Synthesis of the gCN/W_2O_6 nanocomposite through a single step process of instu-polymerisation

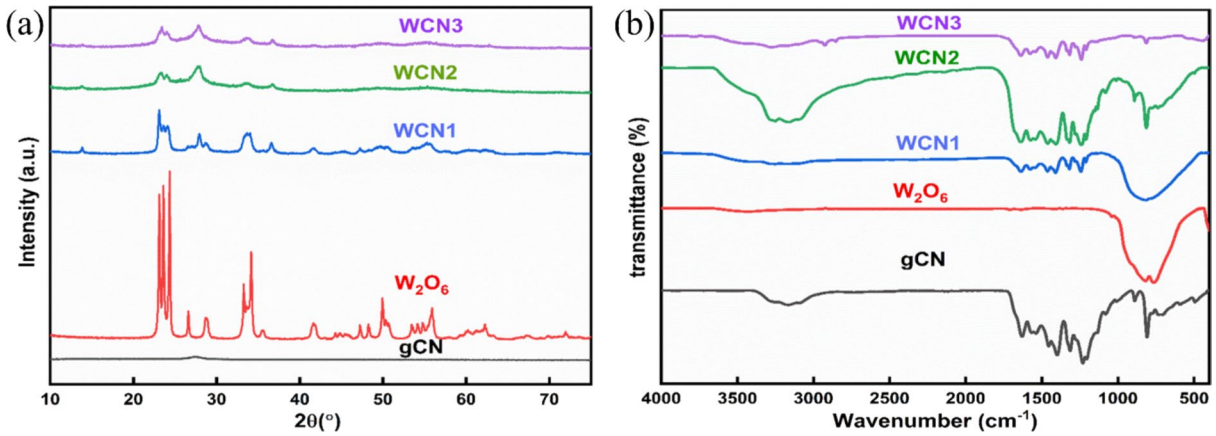

Fig. 2 **a** XRD patterns of gCN, W_2O_6, WCN1, WCN2, and WCN3 composites, **b** FT-IR spectra of pure gCN, W_2O_6, WCN1, WCN2, and WCN3 composites

Photocatalytic activity investigation

In a visible light radiation photocatalytic experiment, several solutions containing organic pollutants were examined to a 200 W bulb in order to assess photocatalytic degradation (Paul et al. 2020b). Each experiment pollutant solution and photocatalyst were secured in dark and stirred with a magnetic stirrer for 30 min in order to reach adsorption–desorption equilibrium. Afterwards, the insoluble photocatalyst particles were separated out by centrifuging the 2 mL solution at regular intervals using a syringe. Using a UV–vis spectrophotometer, the wavelength maxima of absorbance (λ max) was measured at roughly 656 nm. The filtrate concentrations were then determined using Eq. (1).

$$\% \text{ Degradation} = C_o - C_t/C_o \times 100 \quad (1)$$

Consequently, the initial concentrations of pollutants are represented by C_o and C_t is the concentration of pollutants at time t.

The adsorption process significantly impacts dye removal from aqueous solutions. In the dark conditions, i.e., absence of light, the major dye removal is due to the adsorption process (Karimi et al. 2023). During adsorption, dye molecules adhere to the surface of an adsorbent material (Akbari Beni et al. 2024). The adsorption process is generally characterized by a rapid initial uptake of the dye, followed by a slower phase as the available adsorption sites become occupied (Haghbin et al. 2024). It is possible for dyes to be removed simultaneously through adsorption and photocatalytic degradation, a process that combines the strengths of both techniques (Zauška et al. 2024). Adsorption involves the physical or chemical attachment of dye molecules to the surface of an adsorbent material, effectively concentrating the dyes and removing them from the solution (Ranjbari et al. 2023). When these two processes are integrated, the adsorbent material can capture the dye molecules, bringing them into close contact with the photocatalyst. This proximity enhances the efficiency of photocatalytic degradation, as the dye molecules are more readily available for interaction with the reactive species generated.

Results and discussion

Characterization

XRD analysis

Figure 2a displays the samples XRD patterns. Two large peaks can be seen in the synthesized gCN XRD pattern at 2° = 13.6 and 27.7°. The foundation of gCN is known to be tri-s-triazine building blocks (Singh et al. 2019). The interlayer stacking of aromatic systems is responsible for the strongest peak at 27.7°, which is located near graphite peak position (002). Compared to crystalline gCN, which has an interplanar distance of 0.34 nm, the aromatic units have an estimated interplanar distance of 0.327 nm. In the former scenario, this is explained by greater binding between the layers and electron localization. Interlayer stacking is connected to the tiny angle peak at 13.6°, or 0.671 nm. The fact that this distance (0.713 nm) is less than the size of a tris-s-triazine unit suggests that the structure contains a tiny tilt angularity (Li et al. 2021). The peaks attributed to gCN grew

weaker as the composite samples W_2O_6 level increased. The peak at 27.7° in the XRD patterns of the WCN samples is difficult to identify. The gCN sheet exfoliation causes the WCN samples specific surface area to increase if the interlayer stacking is not maintained. A monoclinic structure can be identified by W_2O_6 XRD characteristics.

FTIR analysis

The manufactured samples functions and the W_2O_6@gCN composite structure, as depicted in Fig. 2b, were examined using FTIR. The O–W–O stretching vibrations are responsible for the peaks in the W_2O_6 spectrum that are seen between 600 and 900 cm^{-1}. There are three distinct bands in the gCN spectrum (Safaei et al. 2018). This broad band is ascribed to the N–H stretching vibrations and is situated between 3000 and 3660 cm^{-1}. A second band, seen between 1250 and 1668 cm^{-1}, is consistent with the C–N heterocycles usual stretching vibration. Furthermore, the band of 812 cm^{-1} is attributed to the triazine skeleton bending modes.

The W_2O_6@gCN hybrids FT-IR spectra demonstrate the distinctive qualities of both W_2O_6 and gCN, demonstrating the semiconductors good coupling (Zwane et al. 2023). Strong peak intensities (707 cm^{-1} and 980 cm^{-1}) were seen as the percentage weight of W_2O_6 in the composite increased. Because the bands of W_2O_6 overlap, the peak at 776 cm^{-1} in the WCN semiconductor was gradually diminished (Rajesh et al. 2022). In the WCN composites, the peak at 776 cm^{-1} gradually decreased, presumably as a result of the overlapping W_2O_6 bands. The decrease in intensity between the C and N atoms indicated a contact between gCN and W_2O_6. The efficacious anchoring of W_2O_6 on gCN is demonstrated by the presence of both W_2O_6 and gCN features in the spectra of W_2O_6@gCN nanocomposites.

Surface morphology analysis

The developed photocatalyst gCN FE-SEM images are shown in Fig. 3a. Graphitic carbon nitride (g-C_3N_4) typically exhibits a layered, sheet-like structure with a smooth and uniform surface when observed under a Scanning Electron Microscope (SEM). In contrast, SEM images of a nanocomposite composed of g-C_3N_4 doped with tungsten oxide (W_2O_6) reveal a more complex morphology (Mamba and Mishra 2016). The g-C_3N_4 sheets are interspersed with irregularly shaped W_2O_6 nanoparticles or nanorods, resulting in a rougher texture and potential surface structural modifications. The presence of consistent dark patches in the SEM images of the WCN nanocomposite indicates uniform distribution of W_2O_6, as the higher molecular weight of W_2O_6 compared to g-C_3N_4 causes the W_2O_6 nanoparticles to appear darker. WCN photocatalyst is made up of thin, loose sheets that have widths and lengths up to a specific nanometer, as seen in Fig. 3b. The sheets of WCN combine to form a huge, bulky structure of amygdaloidal rock shape.

The obtained pure WCN2 samples were subjected to EDAX (Energy Dispersive X-Ray Analysis) in order to analyze each sample composition at a more fundamental level. Graphitic carbon nitride is primarily composed of carbon (C) and nitrogen (N) atoms, forming a layered structure with strong covalent bonds. The elemental mapping of gCN typically reveals a uniform distribution of these two elements, highlighting their presence and arrangement within the material. This composition is crucial for its applications in photocatalysis and energy storage due to the electronic properties imparted by the C-N network (Mousavi et al. 2016). Elemental mapping of WCN2 is as seen in Fig. 3c–f, C, N, O, and W are present and there are very few impurities. One can observe peaks in an EDAX spectrum (Fig. 4b) that match the components of the actual composition of WCN2. Figure 4f shows the percentage evaluation of the WCN2 components.

Thermogravimetric analysis

The thermograms of virgin gCN and composites of WCN2 are displayed in S1. Throughout the heating program, pure gCN showed very little weight loss, indicating good thermal stability. Alaghmandfard and Ghandi (2022) Comparable outcomes to those mentioned by other writers. At roughly 650 °C, gCN demonstrated total breakdown in the meanwhile. For the hybrid, there was a minor movement in the decomposition temperature toward higher values, suggesting an improvement in thermal stability (Arora et al. 2022). This was explained by W_2O_6 primary function in stabilizing the nanocomposite, which also supported W_2O_6 incorporation into gCN. One possible explanation for the hybrids enhanced heat stability is the catalytic oxidation of W_2O_6.

XPS analysis

XPS examination was used to examine the materials chemical environments and oxidation states (Chand and Mondal 2023); the findings are displayed in Fig. 4. The synthetic

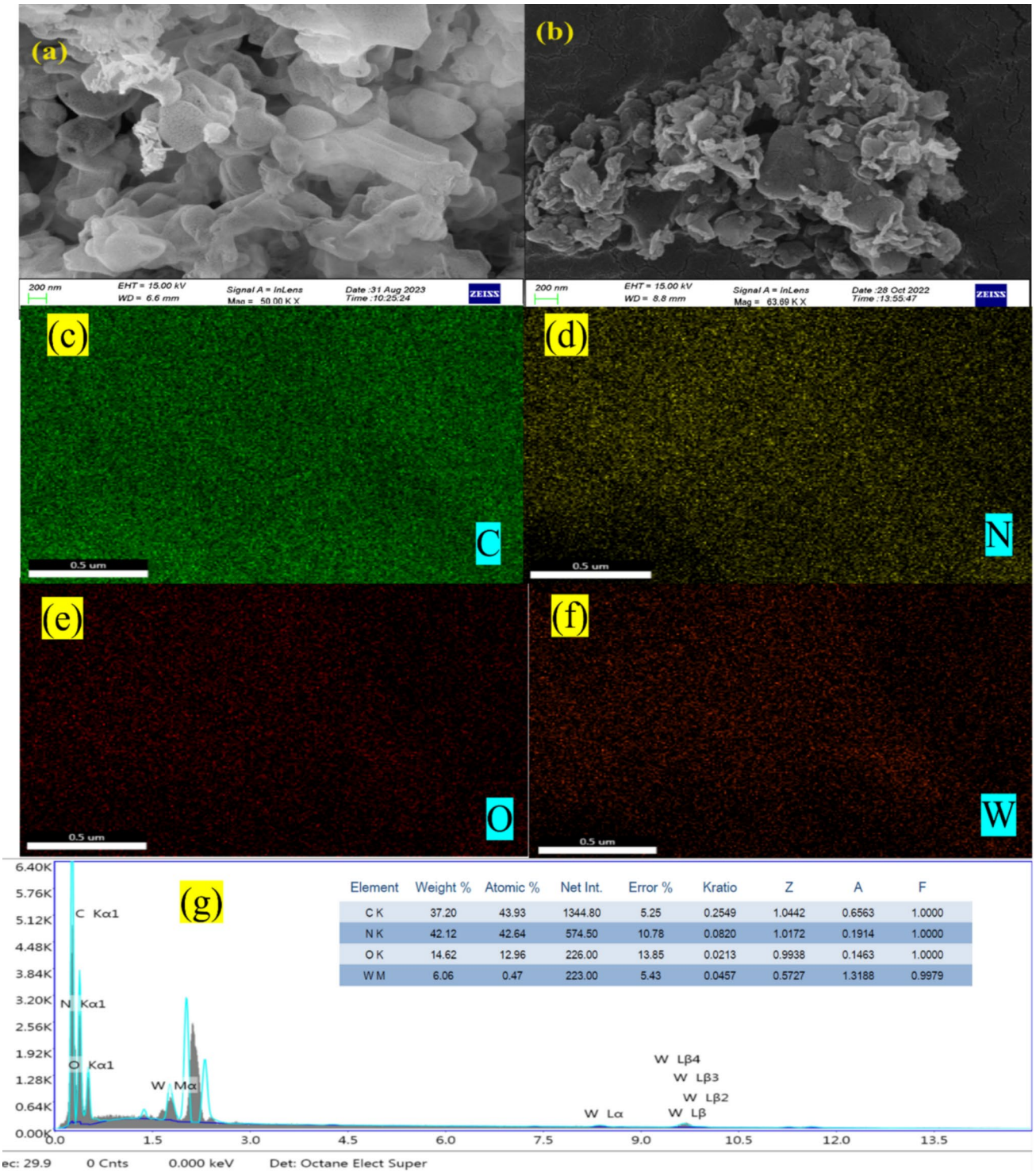

Fig. 3 **a, b** SEM images for the synthesized gCN, WCN at 200 nm magnification. EDAX elemental mapping of **c** Carbon, **d** Nitrogen, **e** Oxygen, **f** Tungsten. **g** EDAX spectra of WCN nanoparticles with Percentage analysis of WCN elements

photocatalyst WCN2 XPS survey is displayed in Fig. 4a–d, highlighting the many elements present in the material, including O, N, C, and W. Figure 4a–d also shows high-resolution XPS spectra, with C 1s, N 1s, O 1s, and W 4f, respectively. Two peaks in the C 1 s spectra, located at 276.4 eV and 278.1 eV, are indicative of the C–C coordination between the C=O and surface adventitious carbon groups. A prominent N 1 s peak is seen at 387.6 eV in

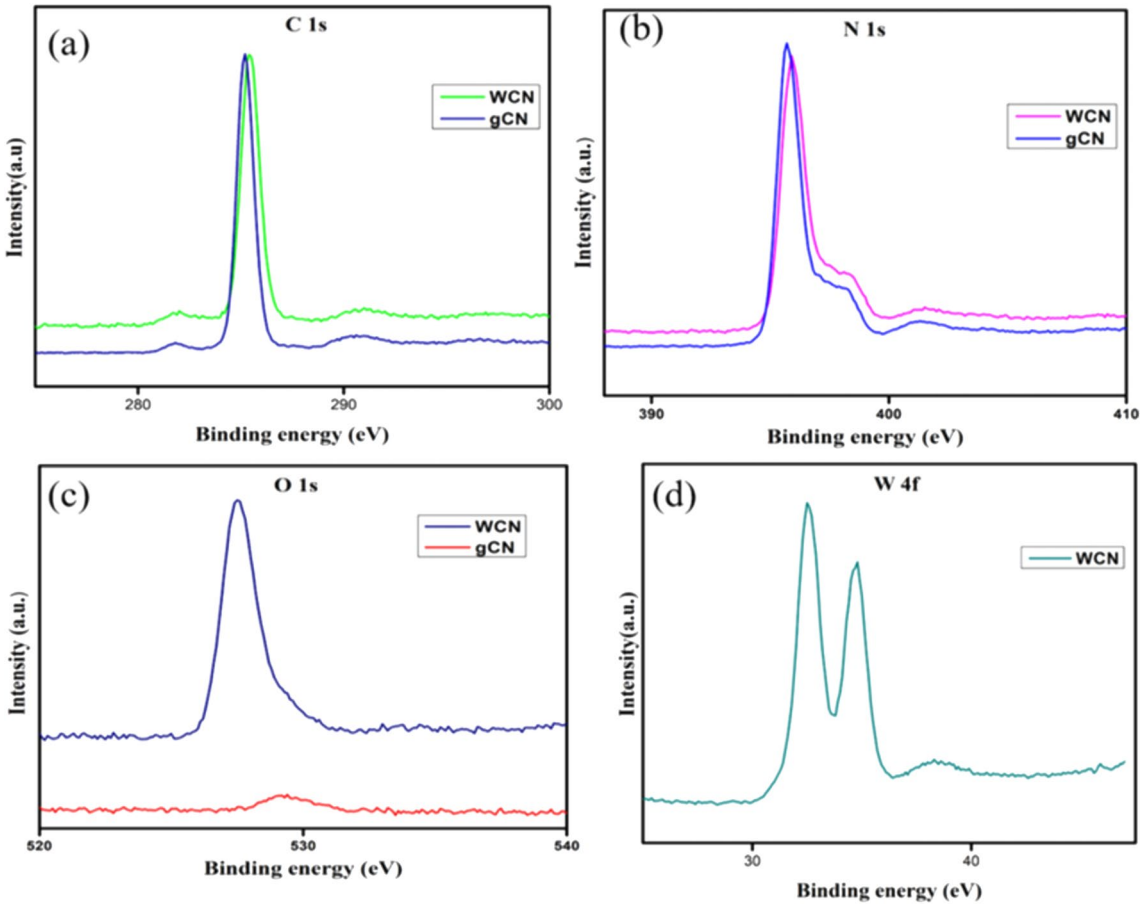

Fig. 4 WCN2 XPS spectra are as follows: analyze (**a**), C1s (**b**), N1s (**c**), O1s (**d**), and W 4f

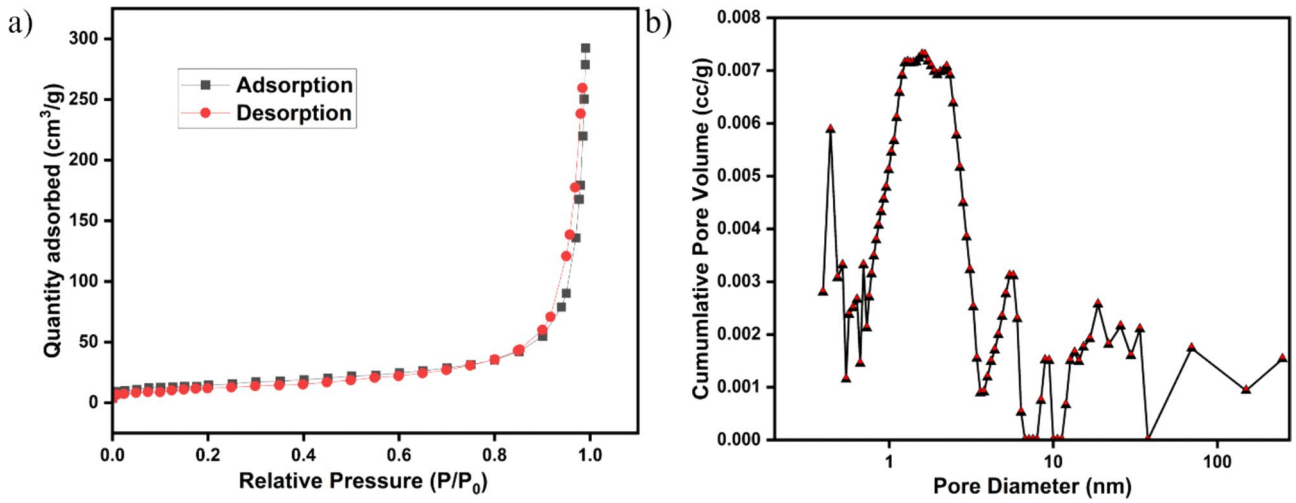

Fig. 5 **a** N_2 adsorption–desorption isotherm. **b** BJH plot for WCN2

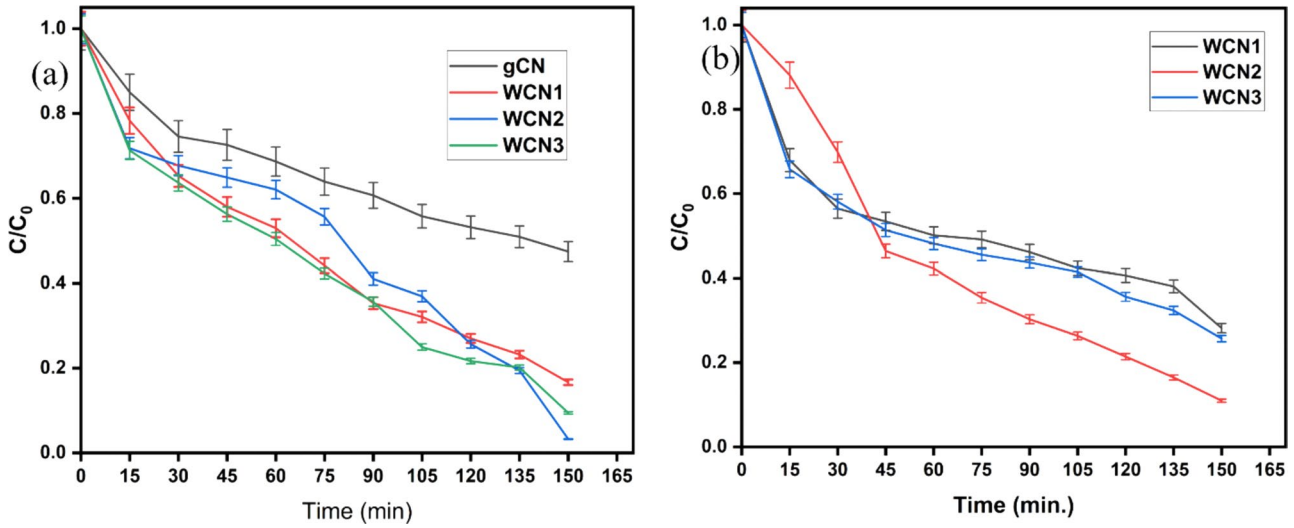

Fig. 6 C/C_0 versus Time Graph for **a** Methylene Blue and **b** Methyl Orange

Fig. 4b, and it is thought to be caused by an aromatic N that has hybridized with two Cs in a triazine ring. One prominent peak at 532.8 in the O 1s high-resolution spectrum is attributed to the metal oxide. The interaction energy of the W peak in the WCN W 4f spectrum, which is situated at 35.69 eV and 36.29 eV, is attributed to the + 6 oxidation state W 4f7/2 and W 4f5/2 spin orbits, respectively (Zwane et al. 2023). The components presence in the hybrid material attests to W_2O_6 and gCN successful integration.

BET studies

The BET isotherms of WCN2 are shown in Fig. 5. The Nitrogen gas adsorption–desorption isotherms at 77 K temperature (Zhang et al. 2021) were used to estimate the surface area and pore size distribution of WCN2. Figure 5a shows the type IV adsorption–desorption isotherm. Figure 5a indicates the mesoporous behaviour of the WCN2 in a wide range of relative pressure of 0.25–0.95. Figure 5b displays an adsorption curve BJH plot for pore size distribution. The pore size of WCN2 majorly concentrates in regions below 40 nm. WCN2 has an average pore size of 31.865 nm and an estimated specific surface area of 52.011 m^2/g with a pore volume of 0.4143 cc/g. The BET study confirms the particles mesoporous nature, with a large surface area and fine pore size organized to perform for better conductivity.

UV–Vis analysis

The optical band gap can be determined using the Davis and Mott relation for direct transitions, expressed as $(\alpha h\nu)^2 = k(h\nu - Eg)$, where α represents the absorption coefficient, Eg is the optical band gap, and k is a proportionality constant (Rao et al. 2023). By extrapolating the linear portion of the plot to the point where absorption equals zero, the band gap energy of the composites can be accurately obtained. S 6 illustrates the Tauc plot for the WCN nanocomposites. The band gap energies for gCN and WCN2 are found to be 2.72 eV and 2.57 eV, respectively. Notably, WCN2 exhibits the smallest band gap, indicating its superior performance as a semiconductor material among the composites analyzed.

Photocatalytic analysis

The generated materials were subjected to photocatalytic degradation toward methylene blue (MB) and methylene orange (MO) dye, as shown in S2 Samples of WCN2 performed better in terms of photocatalytic activity, as seen in S2. The interaction of the dye molecules with the photocatalyst determines the photocatalytic activity. MB is a cationic dye, whereas MO is an anionic dye that may exhibit distinct adsorption behavior on the photocatalyst surface. Higher degradation rates may result from a photocatalyst that has a positive surface charge because it can absorb MO more successfully. Because oxygen vacancies and surface imperfections in the photocatalyst promote the production of additional reactive oxygen species (ROS),

such as hydroxyl radicals (·OH), which are essential for MB chromophore breakdown, they can greatly accelerate the degradation of MB. MO is a relatively complicated anionic azo dye that has an azo bond (–N=N–) that is often difficult to break (Zhou et al. 2021). The primary process by which MO degrades is the breaking of the azo bond, which produces smaller aromatic amines. The chromophore of MB, a cationic dye with a less complex molecular structure, is an aromatic thiazine ring. This ring structure must normally be broken down in order for MB to degrade; this process can happen more quickly and is frequently simpler than the azo bond cleavage in MO (Rao et al. 2023). Each distinct composite dye degradation potential was examined and contrasted with that of gCN-pure and WCN S2. It was found that WCN2 has the highest efficiency was 98.8% after 150 min. To destroy MB and MO, three distinct photocatalytic composites of W_2O_6 and gCN in the proportions of WCN1, WCN2, and WCN3 were created. The photocatalytic degradation rate of MB by composites is 52.46% for gCN, 86.4% for WCN1, 98.8% for WCN2, and 91.2% for WCN3 after 150 min in visible light (400–800 nm) S2. For MO, the degradation rate by composites is 72.9% for WCN1, 89.7% for WCN2, and 83.6% for WCN3, respectively S3. The capacity of gCN photocatalytic degradation is increased by the lowered or tiny band gap, which divides the photoinduced electrons and holes (Zhou et al. 2021). A substance known as a photocatalytic material has the ability to create holes and electrons when exposed to appropriate levels of light. Figure 6a, b represents the C/C_0 graphs for dye degradation potential of all different composites.

Kinetic studies

The degradation of MO and MB followed first-order kinetics, based to the kinetic study. Understanding first-order kinetics principles, data representation, and the meaning of R-squared values, intercepts, and slopes in the kinetic plot (Fig. 7a, b) are all necessary for analyzing the first-order kinetics of the degradation of Methylene Blue and Methyl Orange (Ahluwalia et al. 2016). An extensive comprehension of these chemicals breakdown process will be possible thanks to our analysis. This number represents the linear regression goodness of fit.

We have the following data for Methylene Blue and Methyl Orange:

Methylene Blue**:** $R^2 = 0.99452$, Intercept = − 0.08803, Slope = − 0.01011.

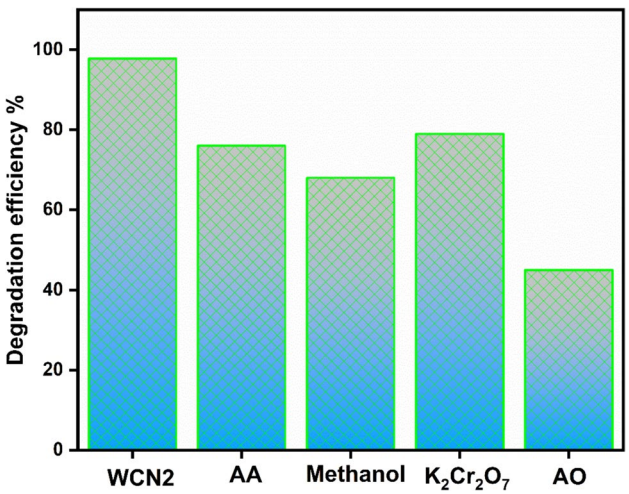

Fig. 8 Effect of electron, hole, $O2^{\cdot-}$ and $^{\cdot}OH$, and scavengers on MB dye degradation for 150 min of irradiation

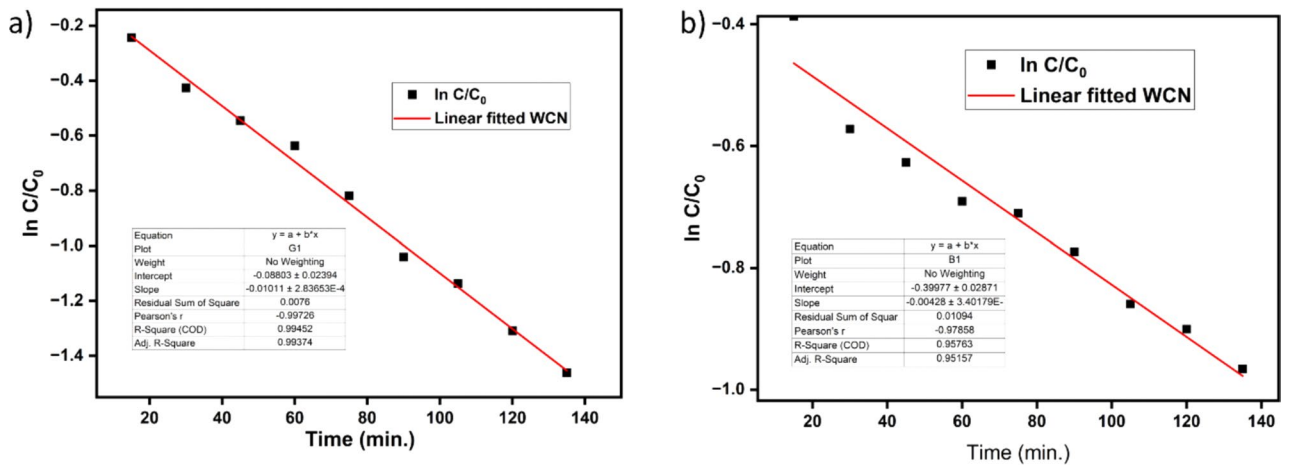

Fig. 7 First order Kinetics of dye degradation of MB and MO for WCN nanocomposites

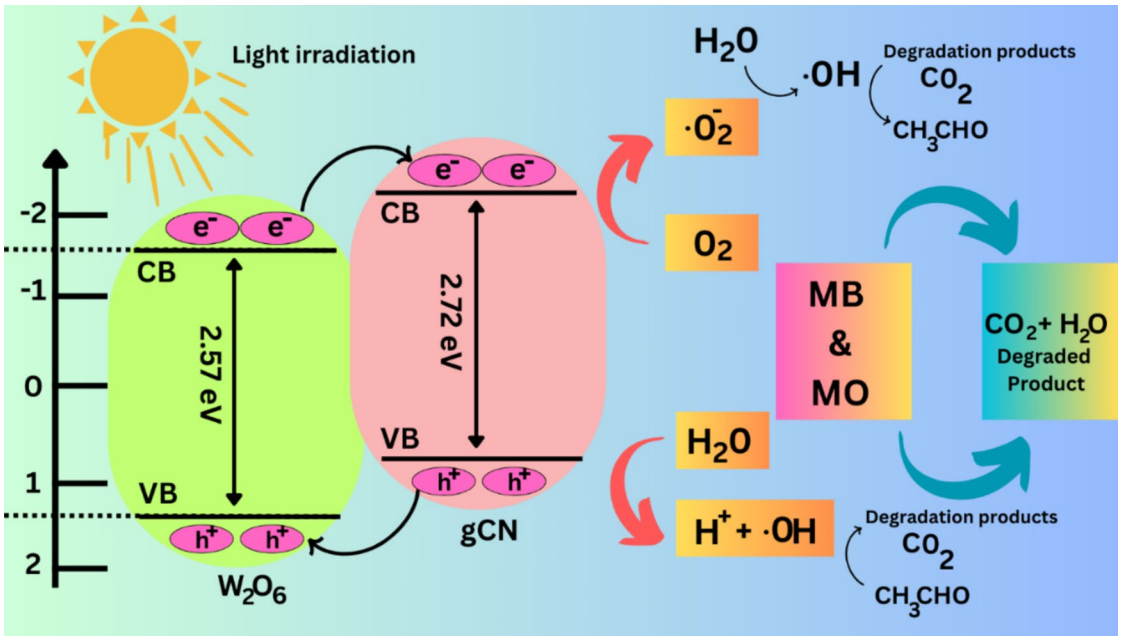

Fig. 9 The degradation process of W_2O_6 and gCN composite under visible light irradiation as photocatalytic

Methyl Orange: $R^2 = 0.95763$, Intercept = − 0.39977, Slope = − 0.00428.

Scavenger test

The free radical mechanism was followed in the dyes breakdown. Water and CO_2 were the byproducts of colour breakdown (Al Jahdaly et al. 2021). The results of the scavenger hunt proved this. The reactive oxygen species (ROS) involved in the photocatalytic process were found using a scavenger test. These assays aid in the comprehension of the function of native oxygen species, including singlet oxygen ($^1O_2$), superoxide anions ($O_2^{\cdot-}$), and hydroxyl radicals ($^{\cdot}OH$), in the breakdown of pollutants and other photocatalytic processes. With more photocatalytically reactive sites available, the WCN2 sample with a high surface area may produce more photogenerated electrons and less photogenerated charge carrier recombination. Using a UV–vis spectrometer and 0.1 mM ascorbic acid (AA), 10 mM methanol (M), 10 mM potassium dichromate ($K_2Cr_2O_7$), and 10 mM ammonium oxalate (AO) as $O_2^{\cdot}$, $^{\cdot}OH$ radicals, e^-, and h^+ scavengers, respectively, trapping studies were conducted to demonstrate the role dynamic species played in the degradation of MB dye after 150 min of exposure to visible light. Figure 8 demonstrates how AO dramatically decreased photoactivity, suggesting that h^+ was the main factor in the photodegradation process. The fact that methanol and AA hindered photoactivity to a lesser extent indicates that $O_2^{\cdot}$ and $^{\cdot}OH$ reactive species are not the main agents involved in photodegradation. However, the absence of any blockage to photoreduction in the presence of $K_2Cr_2O_7$ suggests that e^- had little effect on photodegradation.

Possible photocatalytic degradation mechanism

The observations showed that the main species destroying Methylene orange (MO) and Methylene blue (MB) were superoxide and hydroxyl radicals, and holes took part in the photodegradation process as well (Yoon et al. 2017). The photocatalytic mechanism employing synthesized material was predicted, along with the valence band and conduction band calculations as shown in Fig. 9. The band gap of gCN and W_2O_6 was 2.72 eV and 2.57 eV, respectively, according to UV–visible measurements. Strong oxidants known as hydroxyl radicals ($^{\cdot}OH$) are known to contribute to the breakdown of Methylene blue and Methylene orange when water vapor is present in the atmosphere. The following reactions can convert water molecules into $^{\cdot}OH$ at the photocatalyst surface through interactions with photogenerated holes (h^+) or superoxide radicals (O^{2-}):

$$h^+ + H_2O \rightarrow^{\cdot} OH + H^+$$

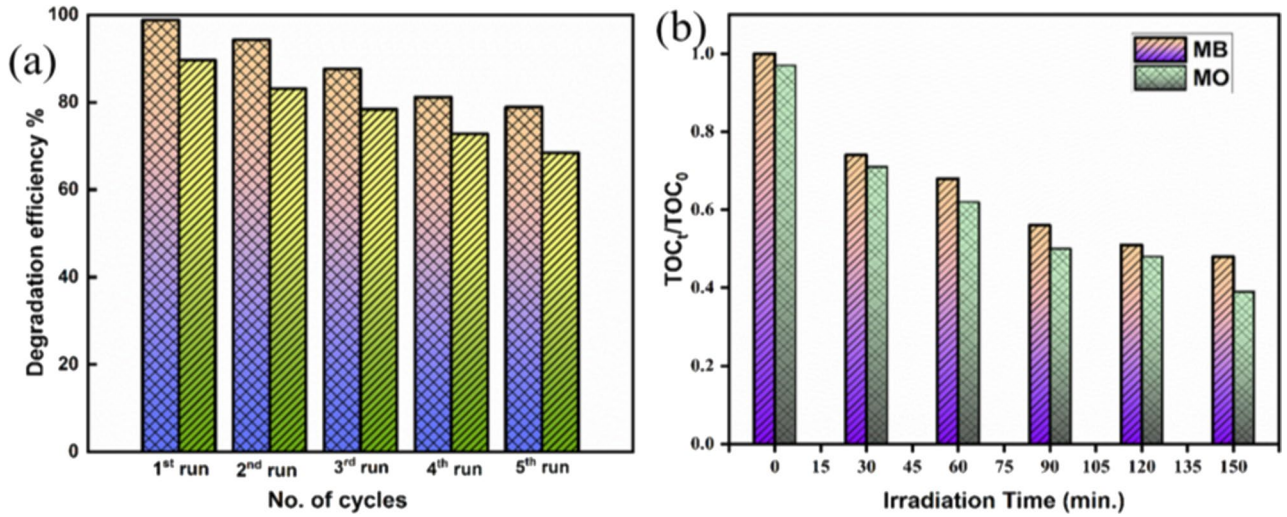

Fig. 10 **a** Using the WCN2 photocatalyst, stability and reusability were assessed. **b** Using WCN2 composite, the TOC removal rate was 10 PPM for MB and MO

$$2O^{2\cdot-} + 2H_2O \rightarrow 2^{\cdot}OH + 2OH^- + O_2$$

Furthermore, it is well known that hydrogen peroxide (H_2O_2) is a potent oxidant. The following reaction can convert oxygen molecules into H_2O_2 at the W_2O_6 surface by interaction with photoexcited electrons:

$$O_2 + 2H^+ + 2e^- \rightarrow H_2O_2$$

As illustrated in Scheme 1, when visible light was applied to the gCN/W_2O_6 (WCN) composite samples, gCN and W_2O_6 valence bands (VB) and conduction bands (CB), respectively, were stimulated to receive electrons. This resulted in holes being left in the VB in both materials (Chaudhary et al. 2021). Diffuse electrons from the photoinduced gCN reach the surfaces, where they combine with O_2 to create O^{2-}. Jointly with photoinduced electrons in the W_2O_6, electrons that were transferred through the CB of gCN to the CB of W_2O_6 react with O_2 to produce H_2O_2 mainly to its high oxidation potential (+ 3.15 V vs. SHE), some photogenerated holes in W_2O_6 diffuse to its surfaces where they either directly destroy the MB and MO incorporated in the W_2O_6 particles or react with surface-bound H_2O to produce the hydroxyl radical species, $^{\cdot}OH$ (Murugalakshmi et al. 2020). The VB of gCN (+ 1.57 V vs. SHE) receives additional photogenerated holes in W_2O_6 that are passed on from the VB of W_2O_6 (+ 3.15 V vs. SHE). The MB and MO that is absorbed on the gCN particles is directly degraded by these transferred holes as well as the photogenerated holes in gCN. The gCN and W_2O_6 surface generates active oxygen species, which are liberated and diffuse through the gas phase, oxidizing the MB and MO dyes (Sher et al. 2021). These species include $^{\cdot}OH$, O^{2-}, and H_2O_2.

In spite of effective separation of produced charge carriers and the capacity to release electrons with strong reduction potential and holes with better oxidization ability, the Z-scheme mechanism greatly enhance the capability of photocatalyst (Zhang et al. 2021). S5 demonstrates the similarity between the produced WCN and other gCN materials reported by other authors well illustrated with the help of 3D diagram S4.

Reusability experiment

Reviewing the reusability and durability of a semiconductor has a significant impact on its practical application. Thus, by recurring the degradation experiments of MB and MO, the sustainability of the fabricated material as the photocatalytic was examined and the results are shown (Chen et al. 2021). Before the photocatalytic experiment and after every cycle, the photocatalyst was thoroughly cleaned with water. To assess the manufactured WCN2 sample reusability, five cycles of recycling experiments were conducted. The dynamic photo catalysts were again collected and used in the following cycle under identical conditions following each photocatalytic testing run. Throughout every test run, it was found that the photoactivity efficiency remained almost

consistent. Small reduction in activity for every cycle could be attributed to the photocatalyst losing its activity during test runs. WCN2 after five cycles demonstrates that the composite morphology did not significantly alter, which is in excellent agreement with the synthetic composites stability as shown in Fig. 10a.

Total organic carbon

Apart from the aforementioned features, the process of photocatalysis observed in the beginning of experiment indicated that WCN2 has the ability to mineralize MO and MB. Thus, during the degradation of the MO and MB dyes, the total organic carbon (TOC) values were determined in order to evaluate the mineralization capacity of WCN2. As seen in Fig. 10b, about half of the total TOC was lost during photodegradation, despite the fact that both MO and MB, two broad-spectrum anionic and cationic dyes, had proved to be environmentally stable (Liu et al. 2021a). Throughout the timeframe, there is a clear downward trend in TOC_t/TOC_0 that was obtained using WCN2. In order to remove intermediates that could endanger the environment and ecosystem, wastewater containing dyes must be treated quickly by mineralization (Liu et al. 2019).

Conclusion

A simple sonication and calcination process was used to create a heterojunction with Z-scheme photocatalyst made from W_2O_6 and gCN. The interaction between gCN and W_2O_6 enhanced the dyes and organic pollutants photocatalytic performance because of the enhanced migration of photogenerated holes and electrons, resulting in decline in gCN conduction band abilities and severe oxidation from W_2O_6 valence band abilities. The hybrid photocatalysts ability to separate electron/hole pairs and transmit charge across the interface more quickly were further validated by the electrochemical analysis. The degradation of methylene orange and methylene blue occurred quickly. $^{\cdot}OH$, O^{2-}, and h^+ supported the hybrid WCN surface degrading process, with $^{\cdot}O_2$ and $^{\cdot}OH$ being the most prevalent species. After being utilized five times, the photocatalytic nanoparticles continued to exhibit significant photoactivity of over 85%, suggesting a high degree of stability and repeatability. Following the deterioration process, the photocatalyst's chemical structure did not charge. The photodegradation process of WCN is characterized by a Z-scheme mechanism, which is supported by the trapping experiments and characterization analysis. Accordingly, it is substantiated that the WCN heterojunction holds promising potential as a proficient visible-light photocatalyst for the degradation of dyes in aqueous environments.

Supplementary Information The online version contains supplementary material available at https://doi.org/10.1007/s13762-024-06127-0.

Acknowledgements AS is highly thankful to Science and Engineering Board (SERB), Department of Science and Technology (DST), Government of India for providing research fellowship under the SERB International Research Experience (SIRE) program (ref. no. SIR/2022/001589). SPN and AS are thankful to Science and Engineering Board (SERB), Department of Science and Technology (DST), Government of India for providing research fund under the SERB State University Research Excellence (SERB-SURE) program (ref. file no. SUR/2022/004191).

Author contributions Vikrant Singh Rao: measurements, data validation, data analysis, writing original draft. Anshu Sharma and S. P. Nehra: supervision, project management, concepts, methodology and writing-review and editing.

Availability of data and materials The data are available on request.

Declarations

Conflict of interest We declare that we have no significant competing financial, professional, or personal interests that might have influenced the performance or presentation of the work described in this manuscript. We have no conflicts of interest to disclose.

Ethical approval For this type of study formal consent is not required.

References

Ahluwalia S, Prakash NT, Prakash R, Pal B (2016) Improved degradation of methyl orange dye using bio-co-catalyst Se nanoparticles impregnated ZnS photocatalyst under UV irradiation. Chem Eng J 306:1041–1048. https://doi.org/10.1016/j.cej.2016.08.028

Akbari Beni F, Izadpanah Ostad M, Niknam Shahrak M, Ayati A (2024) Unveiling the remarkable simultaneous adsorption-photocatalytic potential of Ag nanoparticles-anchored phosphotungestic acid loaded ZIF-8 for Congo red removal. Environ Res 252:119049. https://doi.org/10.1016/j.envres.2024.119049

Al Jahdaly BA, Al-Radadi NS, Eldin GMG et al (2021) Selenium nanoparticles synthesized using an eco-friendly method: Dye decolorization from aqueous solutions, cell viability, antioxidant, and antibacterial effectiveness. J Mater Res Technol 11:85–97. https://doi.org/10.1016/j.jmrt.2020.12.098

Alaghmandfard A, Ghandi K (2022) A comprehensive review of graphitic carbon nitride (g-C3N4)–metal oxide-based nanocomposites: potential for photocatalysis and sensing. Nanomaterials. https://doi.org/10.3390/nano12020294

Arora R, Dhanda M, Yadav M et al (2023) Bi-functionality of Coral reef-like nano-range composites fabricated as g-C3N4/ppy/PSS for efficacious electrochemical super-capacitive energy accumulation and dye depletion. Solid State Ionics 403:116402. https://doi.org/10.1016/j.ssi.2023.116402

Arora R, Nehra SP, Lata S (2022) In-situ composited g-C3N4/polypyrrole nanomaterial applied as energy-storing electrode with ameliorated super-capacitive performance. Environ Sci Pollut Res. https://doi.org/10.1007/s11356-022-21777-8

Bahuguna A, Choudhary P, Chhabra T, Krishnan V (2018) Ammonia-doped polyaniline-graphitic carbon nitride nanocomposite as a heterogeneous green catalyst for synthesis of indole-substituted 4 H-chromenes. ACS Omega 3:12163–12178. https://doi.org/10.1021/acsomega.8b01687

Chand S, Mondal A (2023) g-C3N4/ZrO2 composite material: a pre-eminent visible light-mediated photocatalyst for rhodamine B degradation in the presence of natural sunlight. Ceram Int 49:5419–5430. https://doi.org/10.1016/j.ceramint.2022.10.065

Chaudhary H, Chaudhary K, Zulfiqar S et al (2021) Fabrication of reduced Graphene Oxide supported Gd3+ doped V2O5 nanorod arrays for superior photocatalytic and antibacterial activities. Ceram Int 47:32521–32533. https://doi.org/10.1016/j.ceramint.2021.08.146

Chen J, Fu X, Chen H, Wang Z (2021) Simultaneous Gd2O3 clusters decoration and O-doping of g-C3N4 by solvothermal-polycondensation method for reinforced photocatalytic activity towards sulfamerazine. J Hazard Mater 402:123780. https://doi.org/10.1016/j.jhazmat.2020.123780

Das D, Banerjee D, Das B et al (2017) Effect of cobalt doping into graphitic carbon nitride on photo induced removal of dye from water. Mater Res Bull 89:170–179. https://doi.org/10.1016/j.materresbull.2017.01.034

Haghbin MR, Niknam Shahrak M, LotfiKatooli L, Mirzaei S (2024) Potential of green-based microporous carbon for advanced water decontamination from azo dyes: experiment and molecular dynamic simulation studies. J Environ Chem Eng 12:111875. https://doi.org/10.1016/j.jece.2024.111875

Huang Y, Chen F, Guan Z et al (2022) S-Scheme BiOCl/MoSe2 heterostructure with enhanced photocatalytic activity for dyes and antibiotics degradation under sunlight irradiation. Sensors 22:1–14. https://doi.org/10.3390/s22093344

Ji J, Bao Y, Liu X et al (2021) Molybdenum-based heterogeneous catalysts for the control of environmental pollutants. EcoMat 3:1–34. https://doi.org/10.1002/eom2.12155

Kamarasu L, Sree Nannapaneni S, Arunachalam S et al (2022) GCN decorated manganese oxide for photocatalytic degradation of methylene blue. Inorg Chem Commun 145:109949. https://doi.org/10.1016/j.inoche.2022.109949

Karimi F, Zare N, Jahanshahi R et al (2023) Natural waste-derived nano photocatalysts for azo dye degradation. Environ Res 238:117202. https://doi.org/10.1016/j.envres.2023.117202

Li L, Feng J, Guo S, et al (2021) Direct Z-scheme GdFeO3 / g-C3N4 heterostructures with outstanding photocatalytic activity. Res Sq 1–11

Li X, Song X, Ma C et al (2020) Direct Z-scheme WO3/graphitic carbon nitride nanocomposites for the photoreduction of CO2. ACS Appl Nano Mater 3:1298–1306. https://doi.org/10.1021/acsanm.9b02083

Liu G, Feng M, Tayyab M et al (2021a) Direct and efficient reduction of perfluorooctanoic acid using bimetallic catalyst supported on carbon. J Hazard Mater 412:125224. https://doi.org/10.1016/j.jhazmat.2021.125224

Liu H, Yu D, Sun T et al (2019) Fabrication of surface alkalinized g-C 3 N 4 and TiO 2 composite for the synergistic adsorption-photocatalytic degradation of methylene blue. Appl Surf Sci 473:855–863. https://doi.org/10.1016/j.apsusc.2018.12.162

Liu Y, Zhu Q, Tayyab M et al (2021b) Single-atom Pt loaded zinc vacancies ZnO–ZnS induced type-V electron transport for efficiency photocatalytic H2 evolution. Sol RRL. https://doi.org/10.1002/solr.202100536

Mamba G, Mishra AK (2016) Graphitic carbon nitride (g-C3N4) nanocomposites: a new and exciting generation of visible light driven photocatalysts for environmental pollution remediation. Appl Catal B Environ 198:347–377. https://doi.org/10.1016/j.apcatb.2016.05.052

Mendoza-Sánchez B, Brousse T, Ramirez-Castro C et al (2013) An investigation of nanostructured thin film α-MoO3 based supercapacitor electrodes in an aqueous electrolyte. Electrochim Acta 91:253–260. https://doi.org/10.1016/j.electacta.2012.11.127

Menon S, Agarwal H, Shanmugam VK (2021) Catalytical degradation of industrial dyes using biosynthesized selenium nanoparticles and evaluating its antimicrobial activities. Sustain Environ Res. https://doi.org/10.1186/s42834-020-00072-6

Mo R, Li J, Tang Y et al (2019) Introduction of nitrogen defects into a graphitic carbon nitride framework by selenium vapor treatment for enhanced photocatalytic hydrogen production. Appl Surf Sci 476:552–559. https://doi.org/10.1016/j.apsusc.2019.01.085

Mousavi M, Habibi-Yangjeh A, Abitorabi M (2016) Fabrication of novel magnetically separable nanocomposites using graphitic carbon nitride, silver phosphate and silver chloride and their applications in photocatalytic removal of different pollutants using visible-light irradiation. J Colloid Interface Sci 480:218–231. https://doi.org/10.1016/j.jcis.2016.07.021

Murugalakshmi M, Mamba G, Muthuraj V (2020) A novel In2S3/Gd2O3 p-n type visible light-driven heterojunction photocatalyst for dual role of Cr(VI) reduction and oxytetracycline degradation. Appl Surf Sci 527:146890. https://doi.org/10.1016/j.apsusc.2020.146890

Nabeel MI, Hussain D, Ahmad N et al (2023) Recent advancements in the fabrication and photocatalytic applications of graphitic carbon nitride-tungsten oxide nanocomposites. Nanoscale Adv 5:5214–5255. https://doi.org/10.1039/d3na00159h

Paul DR, Gautam S, Panchal P et al (2020a) ZnO-modified g-C3N4: a potential photocatalyst for environmental application. ACS Omega 5:3828–3838. https://doi.org/10.1021/acsomega.9b02688

Paul DR, Sharma R, Panchal P et al (2020b) Synthesis, characterization and application of silver doped graphitic carbon nitride as photocatalyst towards visible light photocatalytic hydrogen evolution. Int J Hydrogen Energy 45:23937–23946. https://doi.org/10.1016/j.ijhydene.2019.06.061

Paul DR, Sharma R, Rao VS et al (2022) Mg/Li@GCN as highly active visible light responding 2D photocatalyst for wastewater remediation application. Environ Sci Pollut Res. https://doi.org/10.1007/s11356-022-21203-z

Rajesh M, Yan WM, Yen YK (2022) Solvothermal synthesis of two-dimensional graphitic carbon nitride/tungsten oxide nanocomposite: a robust electrochemical scaffold for selective determination of dopamine and uric acid. J Appl Electrochem 52:1231–1248. https://doi.org/10.1007/s10800-022-01699-6

Ranjbari S, Ayati A, Niknam Shahrak M et al (2023) Design of [BmIm]3PW12O40Ionic liquid encapsulated-ZIF-8 nanocomposite for cationic dye adsorptive removal: modeling by response surface methodology. Ind Eng Chem Res 62:4636–4645. https://doi.org/10.1021/acs.iecr.2c02943

Rao A, Kaushik A, Singh V, Pal S (2024a) Facile and binder free nanoarchitecturing of anode with biocompatible g-C 3 N 4 -PPy for bacterial community enrichment and green energy generation in microbial fuel cells. Appl Energy 376:124250. https://doi.org/10.1016/j.apenergy.2024.124250

Rao VS, Sharma A, Nehra SP (2024b) Photocatalytic activity of selenium decorated graphitic carbon nitride nanocomposites for dye Industries wastewater remediation. Groundw Sustain Dev 27:101317. https://doi.org/10.1016/j.gsd.2024.101317

Rao VS, Sharma R, Paul DR et al (2023) Architecting the Z-scheme heterojunction of Gd2O3/g-C3N4 nanocomposites for enhanced visible-light-induced photoactivity towards organic pollutants degradation. Environ Sci Pollut Res. https://doi.org/10.1007/s11356-023-25360-7

Rattan Paul D, Nehra SP (2021) Graphitic carbon nitride: a sustainable photocatalyst for organic pollutant degradation and antibacterial applications. Environ Sci Pollut Res 28:3888–3896. https://doi.org/10.1007/s11356-020-09432-6

Safaei J, Mohamed NA, Mohamad Noh MF et al (2018) Graphitic carbon nitride (g-C3N4) electrodes for energy conversion and storage: a review on photoelectrochemical water splitting, solar cells and supercapacitors. J Mater Chem A 6:22346–22380. https://doi.org/10.1039/c8ta08001a

Sher M, Khan SA, Shahid S et al (2021) Synthesis of novel ternary hybrid g-C3N4@Ag-ZnO nanocomposite with Z-scheme enhanced solar light-driven methylene blue degradation and antibacterial activities. J Environ Chem Eng 9:105366. https://doi.org/10.1016/j.jece.2021.105366

Sibiya D, Dlamini BC, Malinga SP (2022) Selenium modified graphitic carbon nitride membrane with improved antibacterial properties against Bacillus cereus and Escherichia coli. J Environ Chem Eng 10:108960. https://doi.org/10.1016/j.jece.2022.108960

Singh J, Arora A, Basu S (2019) Synthesis of coral like WO3/g-C3N4 nanocomposites for the removal of hazardous dyes under visible light. J Alloys Compd 808:151734. https://doi.org/10.1016/j.jallcom.2019.151734

Sundaram IM, Kalimuthu S, Ponniah GP (2017) Highly active ZnO modified g-C3N4 Nanocomposite for dye degradation under UV and Visible Light with enhanced stability and antimicrobial activity. Compos Commun 5:64–71. https://doi.org/10.1016/j.coco.2017.07.003

Tanzifi M, Jahanshahi M, Peyravi M, Khalili S (2023) Photocatalytic dynamic membrane containing graphitic carbon nitride/zirconium dioxide nanocomposite for MB and CR dye removal under household LED lamp. J Water Environ Nanotechnol 8:215–228. https://doi.org/10.22090/JWENT.2023.03.002

Tian Y, Jia N, Ma H et al (2021) 0D/3D coupling of g-C3N4 QDs/hierarchical macro-mesoporous CuO-SiO2 for high-efficiency norfloxacin removal in photo-Fenton-like processes. J Hazard Mater 419:126359. https://doi.org/10.1016/j.jhazmat.2021.126359

Tomer VK, Singh K, Kaur H et al (2017) Rapid acetone detection using indium loaded WO3/SnO2 nanohybrid sensor. Sens Actuat B Chem 253:703–713. https://doi.org/10.1016/j.snb.2017.06.179

Tripathi A, Narayanan S (2018) Impact of TiO2 and TiO2/g-C3N4 nanocomposite to treat industrial wastewater. Environ Nanotechnol Monit Manag 10:280–291. https://doi.org/10.1016/j.enmm.2018.07.010

Tripathi RM, Hameed P, Rao RP et al (2020) Biosynthesis of highly stable fluorescent selenium nanoparticles and the evaluation of their photocatalytic degradation of dye. Bionanoscience 10:389–396. https://doi.org/10.1007/s12668-020-00718-0

Yesmin S, Devi M, Dasgupta R, Dhar SS (2022) CoFe2O4 nanocubes over Cu/graphitic carbon nitride as electrode materials for solid-state asymmetric supercapacitors. Chem Eng J 446:136540. https://doi.org/10.1016/j.cej.2022.136540

Yoon M, Oh Y, Hong S et al (2017) Synergistically enhanced photocatalytic activity of graphitic carbon nitride and WO3 nanohybrids mediated by photo-Fenton reaction and H2O2. Appl Catal B Environ 206:263–270. https://doi.org/10.1016/j.apcatb.2017.01.038

Zauška L, Volavka D, Lisnichuk M et al (2024) Tuning the photocatalytic performance of mesoporous silica-titanium dioxide and cobalt titanate for methylene blue and Congo red adsorption/photodegradation: Impact of azo dyes concentration, catalyst mass, wavelength, reusability and kinetic properties. J Photochem Photobiol A Chem. https://doi.org/10.1016/j.jphotochem.2024.115522

Zhang W, Ma Y, Zhu X et al (2021) Fabrication of Ag decorated g-C3N4/LaFeO3 Z-scheme heterojunction as highly efficient visible-light photocatalyst for degradation of methylene blue and tetracycline hydrochloride. J Alloys Compd 864:158914. https://doi.org/10.1016/j.jallcom.2021.158914

Zhou Y, Zeng F, Sun C et al (2021) Gd2O3 nanoparticles modified g-C3N4 with enhanced photocatalysis activity for degradation of

organic pollutants. J Rare Earths 39:1353–1361. https://doi.org/10.1016/j.jre.2021.06.002

Zwane S, Dlamini DS, Mamba BB, Kuvarega AT (2023) Evaluation of the photodegradation of pharmaceuticals and dyes in water using a highly visible light-active graphitic carbon nitride modified with tungsten oxide. Inorg Chem Commun 151:110637. https://doi.org/10.1016/j.inoche.2023.110637